Single-material anomalous Nernst heat-flux sensor enabled by heat-assisted magnetization reversal

Weinan Zhou,[a] Hirofumi Suto, and Yuya Sakuraba

Research Center for Magnetic and Spintronic Materials, National Institute for Materials Science, Tsukuba 305-0047, Japan

Heat-flux sensors based on the transverse thermoelectric phenomenon of anomalous Nernst effect have attracted increasing interest in recent years due to the advantages stemming from simple and planar sensor structures. However, the difference in Seebeck coefficients of the constituent materials makes the sensors also sensitive to in-plane temperature gradient along the wire direction and can give rise to an undesirable offset in the sensor output. In this study, to mitigate this offset, improve structural efficiency, and simplify device fabrication, we propose a single-material anomalous Nernst heat-flux sensor with antiparallel magnetization alignment in neighboring wires. Using heat-assisted magnetization reversal through electric-current-driven Joule heating, we were able to locally control the magnetization and realize such an antiparallel alignment in devices microfabricated from an $L1_0$-FePt thin film with an in-plane magnetic easy axis. Systematic measurements on a single FePt wire showed the conditions of electric current and magnetic field required for heat-assisted magnetization reversal; these conditions were then applied to a Π-shaped FePt element to selectively reverse one half of its magnetization and achieve antiparallel alignment. As a result, the Π-shaped element with antiparallel magnetization exhibits nearly twice the heat-flux sensitivity of a single wire. These results establish heat-assisted magnetization reversal as an effective way to locally control magnetization for constructing offset-free, single-material anomalous Nernst heat-flux sensors.

[a]Electronic mail: ZHOU.Weinan@nims.go.jp

The anomalous Nernst effect (ANE) is a transverse thermoelectric phenomenon observed in magnetic materials, where an electric field is generated perpendicular to both the temperature gradient (∇T) and the magnetization ($\mathbf{M}$). In recent years, the ANE has attracted increasing attention partly due to this transverse geometry: electrical contacts can be arranged orthogonally to the ∇T direction, different from the parallel configuration required for the Seebeck effect (SE).[1–11] This geometry decouples thermal and electrical transport paths and enables simple and planar structures for the ANE-based thermoelectric modules, unlike the three-dimensional structure composed of serially connected p-type and n-type semiconductor pillars used in a SE-based thermoelectric module. These features make the ANE particularly well suited for heat-flux sensors (HFSs), offering flexibility and scalability together with low thermal resistance.[12–16]

To enhance HFS sensitivity, magnetic wires are often connected in series so that the anomalous Nernst voltage (V_{ANE}) adds constructively, forming a meander structure [Fig. 1(a)]. This can be realized by using a nonmagnetic metal as electrodes to connect the magnetic wires [Fig. 1(b)];[12–14] or by using two different magnetic materials with positive and negative anomalous Nernst coefficient (S_{ANE}) as neighboring wires, for which V_{ANE} adds constructively when their $\mathbf{M}$ are in parallel alignment [Fig. 1(c)].[2,16–21] In both cases, however, the neighboring wires consist of different materials and generally possess different Seebeck coefficients (S_{SE}). When the heat flux through the HFS is nonuniform and induces an in-plane component of ∇T along the wire direction, Seebeck voltages (V_{SE}) are generated, leading to a finite ΔV_{SE} within a repeating unit of the meander structure, which superimpose on V_{ANE} and introduces an undesirable offset in the HFS output. Although several approaches have been proposed to mitigate this issue, such as tuning S_{SE} of the materials through multilayer structure[15] or selecting specific material combinations,[22] their versatility is limited and may not be applicable to other materials. An alternative approach is to fabricate the entire meander structure from a single magnetic material while arranging neighboring wires in antiparallel $\mathbf{M}$ alignment [Fig. 1(d)]. In this case, even in the presence of an in-plane component of ∇T, V_{SE} generated in neighboring wires are identical and cancel out, resulting in a vanishing ΔV_{SE} and eliminating the offset in the HFS output. This includes the magneto-Seebeck effect. Previous studies have shown that the Seebeck coefficient of a magnetic material depends on the relative angle between ∇T and $\mathbf{M}$. The measured V_{SE} as a function of magnetic field applied perpendicular to the direction of ∇T

typically exhibits an even dependence on magnetic field, with identical values once **M** is saturated under either positive or negative field.[23,24] In antiparallel **M** alignment, **M** in the neighboring wires is perpendicular to the in-plane component of ∇T, and thus exhibits the same magneto-Seebeck effect. This approach also improves structural efficiency, as all wires contribute constructively to the output, and simplify device fabrication. However, because the width of the wires in a practical HFS typically ranges from tens to hundreds of micrometers, achieving precise local control of **M** without disturbing neighboring wires remains challenging.[2,25,26]

In this study, we propose an anomalous Nernst HFS consisting of a single magnetic material, in which neighboring wires have antiparallel **M** alignment. This alignment is realized using heat-assisted magnetization reversal, which exploits the reduction of coercivity (H_c) with increasing temperature (T) [Fig. 1(e)]. Heat-assisted magnetization reversal has been applied to heat-assisted magnetic recording, where local heating enables the control of **M** in FePt granular films with high magnetic anisotropy using a reduced magnetic field.[27,28] Here, we used FePt with an in-plane magnetic easy axis, and achieved antiparallel **M** by selectively heating one wire via Joule heat induced by flowing an electric current (I) through the wire. Under magnetic field (H) that is sufficient to align **M** at elevated T but insufficient at room T [Fig. 1(e)], only the heated wire undergoes magnetization reversal. By systematically varying I and H, we mapped the conditions for heat-assisted magnetization reversal in a single FePt wire. Then, using a device with a Π-shaped FePt element, we selectively reversed one half of the element and realized antiparallel **M** alignment. The Π-shaped FePt element with antiparallel **M** exhibited nearly twice the HFS sensitivity compared to that of a single FePt wire.

The thin film used in this study was prepared using an ultrahigh-vacuum magnetron sputtering system. The stacking structure was MgO (110) substrate // Cr (1 nm) / Pt (5 nm) / FePt (28 nm). The MgO substrate was first heated to 600 °C to clean the surface, after which the Cr layer was deposited. The substrate temperature was then reduced to 300 °C for the deposition of the Pt and FePt layers. The crystalline structure of the thin film was characterized by X-ray diffraction (XRD) with Cu K_α radiation, and the magnetic properties were characterized using a superconducting quantum interference device. These measurements confirmed that the $L1_0$-FePt layer was epitaxially grown with its magnetic easy axis aligned along the MgO [001] direction (see Supplementary Material for the X-ray

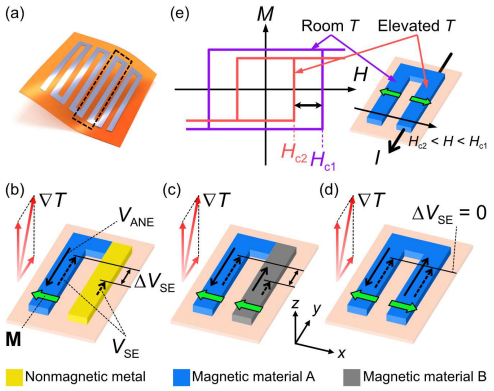

FIG. 1. (a) Schematic illustration of an anomalous Nernst HFS with a meander structure on a flexible substrate. The black dashed square denotes one repeating unit of the meander structure. (b) A repeating unit consists of a magnetic material and a nonmagnetic metal. Only the magnetic material generates a voltage due to ANE (V_{ANE}) under an out-of-plane ∇T. If ∇T also has an in-plane component, voltages due to SE (V_{SE}) emerge in both materials, and a finite ΔV_{SE} is added to V_{ANE} owing to the difference in S_{SE}. (c) A repeating unit consists of two different magnetic materials with positive and negative S_{ANE}. When their magnetizations ($\mathbf{M}$) are aligned parallel along x-axis, the generated V_{ANE} points in opposite directions under an an out-of-plane ∇T, resulting in additive V_{ANE}. However, if ∇T also has an in-plane component, a finite ΔV_{SE} emerges owing to different S_{SE}. (d) A repeating unit consists of a single magnetic material with antiparallel $\mathbf{M}$ on the left and right sides. The generated V_{ANE} is additive, whereas $\Delta V_{\mathrm{SE}} = 0$ under in-plane ∇T owing to identical S_{SE}. (e) Schematic illustration of achieving antiparallel $\mathbf{M}$ alignment by applying an electric current (I) for Joule heat and exploiting different coercivities (H_{c1} and H_{c2}) at room T and an elevated T.

diffraction pattern and M-H curves).[29,30] The composition of the FePt layer was determined to be $Fe_{44}Pt_{56}$ by X-ray flourescence analysis performed on a reference sample without the Cr / Pt buffer layer. For device fabrication, the thin film was patterned into wires and Π-shaped elements by photolithography and Ar ion milling. The wire width was 10 μm, and the width direction was aligned parallel to the MgO [001] direction. The distance between wires was 14 μm for the Π-shaped elements. Ta (2 nm) / Au (150 nm) electrodes were then fabricated

using a lift-off process. The distance between the electrodes on each end of the wires was 100 μm. To apply an out-of-plane ∇T, on-chip heaters were microfabricated on top of the FePt wires and elements to cover them entirely. The heaters were electrically insulated from the FePt by a 10-μm-thick epoxy photoresist (SU-8) layer. After patterning the SU-8 layer and then curing it at 200 °C for 30 min, the on-chip heaters were fabricated from Ta (5 nm) / Au (100 nm) thin film using a lift-off process. The heater wire width and the gap between adjacent wires were both 8 μm, and the heater covered an area of approximately 160 × 160 μm^2 [Fig. 2(a) and Fig. 3(a)]. The measurements were primarily carried out using a prober station equipped with an in-plane electromagnet. The T dependence of the wire resistance (R) was measured using a physical property measurement system (PPMS).

To investigate the conditions for heat-assisted magnetization reversal by Joule heating, we first performed measurements on a device with a single FePt wire. $\mathbf{M}$ reversal was evaluated by measuring V_{ANE} of the wire as a function of H. Figure 2(a) shows a photograph of the device and the measurement configuration. The nanovoltmeter on the right measured V_{ANE}, while the sourcemeter on the right applied I through the wire to generate Joule heat and elevate its T. The sourcemeter on the left applied a heater current to the on-chip heater to generate an out-of-plane ∇T, and the nanovoltmeter on the left was used to estimate the electrical power dissipated in the heater and calculate the heat flux density (J_{Q}) as the power divided by the heater area. Figure 2(b) shows V_{ANE} as a function of H measured with a heater current of 10 mA, corresponding to $J_{\mathrm{Q}} = 331$ kW m^{-2}. Prior to the measurement, $\mathbf{M}$ of the FePt wire was aligned along the $-x$ direction. H was swept from 0 to 240 mT, to -240 mT, and back to 0, as indicated by the numbered arrows in Fig. 2(b). In this case, the $\mathbf{M}$ reversal was driven solely by H, which can be clearly seen as sharp change in V_{ANE}, and H_{c} is obtained to be ~ 167 mT. For heat-assisted magnetization reversal operation, after $\mathbf{M}$ was aligned along the $-x$ direction, we fixed H at a certain positive value (H_{R}) smaller than H_{c}, and applied I through the FePt wire for 1 s. After turning off I and returning H back to zero, the V_{ANE}-H curve was measured to investigate the direction of $\mathbf{M}$, following the same H sequence as shown in Fig. 2(b). This procedure was repeated for different combinations of I and H_{R}, with I ranging from 30 to 50 mA (both polarities) and H_{R} ranging from 15 to 147 mT. We define ΔV_{ANE} as the averaged V_{ANE} value in the range of $0 < \mu_0 H < 150$ mT minus the averaged value at $\mu_0 H > 200$ mT in the initial curve [Fig. 2(f)]. A value of $\Delta V_{\mathrm{ANE}} \sim -5$ μV indicates that the operation was not able to reverse $\mathbf{M}$ [Fig. 2(e)], whereas

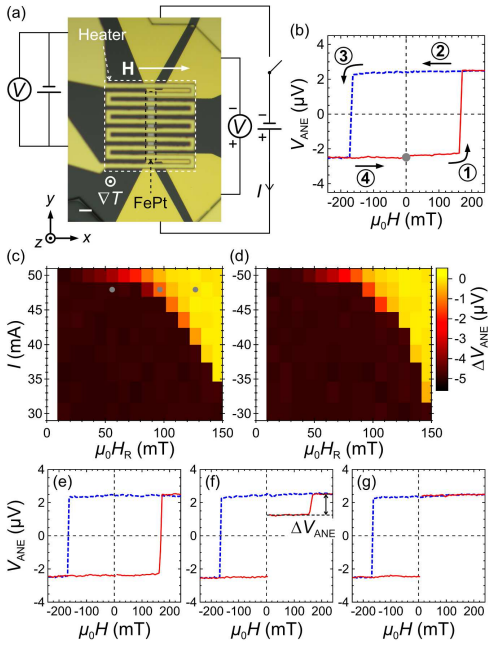

FIG. 2. (a) Photograph of the device containing a single FePt wire, together with a schematic of the measurement configuration. The positive H direction and the ∇T direction are indicated. The scale bar corresponds to 20 μm. (b) V_{ANE} as a function of H measured with a heater current of 10 mA. Numbered arrows indicate the sequence of varying H. (c) Color map of ΔV_{ANE} as a function of H_{R} and positive I, showing the conditions for heat-assisted magnetization reversal of FePt. (d) ΔV_{ANE} as a function of H_{R} and negative I. (e)-(g) V_{ANE}-H curves measured after the operation with $I = 48.0$ mA and (e) $H_{\mathrm{R}} = 56$, (f) 96, and (g) 127 mT, corresponding to the gray dots in (c). ΔV_{ANE} is defined as the averaged V_{ANE} value in the range of $0 < \mu_0 H < 150$ mT minus the averaged value at $\mu_0 H > 200$ mT, as indicated in (f).

$\Delta V_{\mathrm{ANE}} \sim 0$ means that $\mathbf{M}$ was fully reversed and the operation is successful [Fig. 2(g)]. Figure 2(c) (Figure 2(d)) summarizes ΔV_{ANE} as a function of H_{R} and positive I (negative I). Representative V_{ANE}-H curves measured after the operations with $I = 48.0$ mA and $H_{\mathrm{R}} = 56$, 96, and 127 mT are shown in Figures 2(e), 2(f), and 2(g), respectively. The conditions for successful operations, indicated by ΔV_{ANE} being close to zero, appears in the upper-right region of the color map, corresponding to large I and H_{R}. Intermediate ΔV_{ANE}

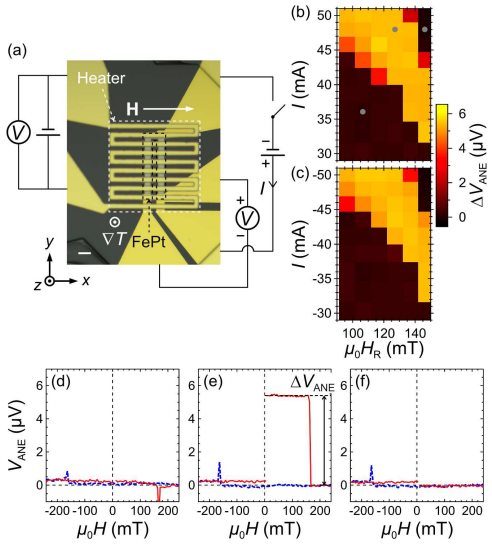

FIG. 3. (a) Photograph of the device containing a Π-shaped FePt element, together with a schematic of the measurement configuration. The positive H direction and the ∇T direction are indicated. The scale bar corresponds to 20 μm. (b) Color map of ΔV_{ANE} as a function of H_{R} and positive I, showing the conditions for achieving antiparallel $\mathbf{M}$ alignment in FePt. (c) ΔV_{ANE} as a function of H_{R} and negative I. (d)-(f) V_{ANE}-H curves measured after the operation with (d) $I = 36.1$ mA and $H_{\mathrm{R}} = 107$ mT, (e) $I = 48.0$ mA and $H_{\mathrm{R}} = 127$ mT, and (f) $I = 48.0$ mA and $H_{\mathrm{R}} = 147$ mT, corresponding to the gray dots in (b).

values at the boundary between successful operation and no $\mathbf{M}$ reversal suggest partial $\mathbf{M}$ reversal [Fig. 2(f)], and this boundary region expanded in H_{R} as I increased towards 50 mA. Although spin torque arising from the spin Hall effect in the Pt layer could, in principle, influence $\mathbf{M}$ reversal of the FePt layer, the very similar color maps obtained for positive and negative I [Fig. 2(c) and 2(d)] suggest that such effect does not play a significant role here, since the polarity of I will determine the direction of spin torque.

Using the conditions obtained for heat-assisted magnetization reversal, we next performed operations on a device with a Π-shaped FePt element to achieve antiparallel $\mathbf{M}$ alignment. Figure 3(a) shows a photograph of the device and the measurement configuration, which is largely the same as that shown in Fig. 2(a), except that the nanovoltmeter on the right

measured the voltage of the entire Π-shaped element, while the sourcemeter on the right was connected only to the right half of the element to generate Joule heat. It is worth noting that no specific thermal isolation measures were implemented, and the Joule heat generated in the wire can propagate to the neighboring wire through the MgO substrate and the SU-8 layer. The same procedure as used for a single FePt wire was repeated here, with I ranging from 30 to 50 mA (both polarities) and H_{R} ranging from 96 to 147 mT. Figure 3(b) (Figure 3(c)) summarizes ΔV_{ANE} as a function of H_{R} and positive I (negative I). The definition of ΔV_{ANE} remains the same. However, a value of $\Delta V_{\mathrm{ANE}} \sim 0$ here indicates that the operation was unsuccessful and $\mathbf{M}$ of the left and right halves were parallel [Fig. 3(d)]. The small peaks observed at $|\mu_0 H| \sim 165$ mT in the V_{ANE}-H curves are attributable to the unsynchronized $\mathbf{M}$ reversal of the element driven by H. By contrast, $\Delta V_{\mathrm{ANE}} \sim 5$ μV indicates that $\mathbf{M}$ of the right half was fully reversed, resulting in antiparallel $\mathbf{M}$ alignment [Fig. 3(e)]. The color maps obtained for positive and negative I [Figs. 3(b) and 3(c)] are very similar, and the conditions for achieving antiparallel $\mathbf{M}$ largely overlap with those observed in Figs. 2(c) and 2(d). Notably, within the area corresponding to antiparallel $\mathbf{M}$ alignment in Figs. 3(b) and 3(c), combinations of $|I| \geq 45.8$ mA and $H_{\mathrm{R}} = 147$ mT result in $\Delta V_{\mathrm{ANE}} \sim 0$, indicating parallel $\mathbf{M}$ alignment. Figure 3(f) shows a representative V_{ANE}-H curve obtained after such an operation, where the disappearance of the small peak at $\mu_0 H \sim 165$ mT indicates that $\mathbf{M}$ of both the left and right halve were reversed. This behavior is likely caused by a combination of increased T in the left half due to heat dissipation from the right half under Joule heating, as well as the reversed magnetic domain propagation under large H. Nevertheless, these results demonstrate that antiparallel $\mathbf{M}$ alignment in a single-material Π-shaped element can be achieved by selective heat-assisted magnetization reversal via Joule heating.

Since the single wire and Π-shaped element of FePt are analogous to the repeating units of HFS shown in Figs. 1(b) and 1(d), respectively, we evaluated and compared their sensitivities by measuring V_{ANE} as a function of J_{Q} [Fig. 4(a)]. The data points represent V_{ANE} measured under zero H, and the dashed lines denote linear fits through the origin, with the slopes corresponding to the sensitivities. The Π-shaped element with antiparallel $\mathbf{M}$ exhibits a sensitivity of 13.0×10^{-3} μV (kW m^{-2})$^{-1}$, nearly twice that of the single wire (7.4×10^{-3} μV (kW m^{-2})$^{-1}$). In contrast, the sensitivity of the Π-shaped element with parallel $\mathbf{M}$ is only -0.2×10^{-3} μV (kW m^{-2})$^{-1}$. This behavior is expected because each half of the Π-shaped

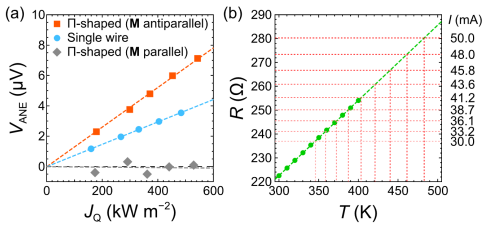

FIG. 4. (a) V_{ANE} under zero field as a function of J_{Q} for devices with a single wire or with a Π-shaped element. The dashed lines denote linear fits through the origin. (b) Measured R of a single FePt wire as a function of T. The green dashed line denotes a linear fit. The red horizontal dashed lines mark the R values measured after operation with various I, while the red vertical dashed lines indicate the estimated wire temperature due to Joule heating.

element has the same length as the single wire and generates a comparable V_{ANE} under the same J_{Q}; the voltages add constructively for antiparallel **M**, while they cancel out for parallel **M**. We also estimated T of the FePt wire after applying I through it for 1 s. For this purpose, we used R of the single FePt wire (shown in Fig. 2(a)) to estimate its T by measuring the T dependence of R. The green data points in Fig. 4(b) were obtained using four-terminal method in a PPMS, which controlled the environment T. The data exhibit a linear relationship, as indicated by the green dashed line. The R values of the single FePt wire measured after applying various values of I for 1 s are shown as horizontal red dashed lines, and their intersections with the green dashed line provide estimates of T due to Joule heating. The maximum T reached after applying 50 mA was estimated to be $\sim$ 483 K, which is lower than the substrate temperature during FePt deposition (573 K). During Joule heating, a temperature gradient may develop within a wire due to the multilayer structure (materials with different electrical resistivities) and asymmetric top and bottom boundary conditions. However, based on our results, such a gradient does not generate a clear effect on the heat-assisted magnetization reversal of the FePt wires, which may be due to the high thermal conductivities of the metallic layers and the small total thickness of the thin film.

These results show that the direction of **M** in the FePt wires can be reversed by the application of I and H via heat-assisted magnetization reversal. However, such a process is not expected to occur during normal HFS operation, which is around room temperature and in the absence of a strong external magnetic field. We measured the M-H curves of

the FePt thin film over a temperature range from 300 K to 400 K with **H** applied along the MgO [001] direction (see Fig. S3 in Supplementary material). Both H_c and saturation magnetization M_s decrease with increasing T. At 300 K, $\mu_0 H_c = 163$ mT, consistent with that of a single FePt wire shown in Fig. 2(b). At 400 K, $\mu_0 H_c$ decreases to 123 mT, which remains significantly higher than magnetic fields typically encountered in daily environments. This value is comparable to the behavior of heat-assisted magnetization reversal with $I =$ 41.2 mA, based on the estimated wire temperature due to Joule heating shown in Fig. 4(b). Although the HFS would lose functionality if the direction of **M** were altered by external conditions (*e.g.*, strong H and/or high T), realignment of **M** would restore device operation.

In conclusion, we propose an anomalous Nernst HFS based on a meander structure fabricated from a single magnetic material, which could mitigate the undesirable SE offset in the HFS output arising from an in-plane component of ∇T. Such an anomalous Nernst HFS relies on antiparallel **M** alignment in neighboring wires of the meander structure, which is realized through selective heat-assisted magnetization reversal induced by electric-current-driven Joule heating. Systematic measurements on a device with a single FePt wire showed the conditions of I and H_R required for **M** reversal. Applying these conditions to a device with a Π-shaped FePt element, we demonstrated antiparallel **M** alignment by selectively heating one half of the element. The Π-shaped element with antiparallel **M** exhibited nearly twice the HFS sensitivity of a single wire. The local **M** control demonstrated here is applicable to other magnetic materials with finite coercivity. These results establish heat-assisted magnetization reversal via Joule heating as a practical and versatile approach for constructing single-material anomalous Nernst HFS, paving the way for wider adoption of HFS and contributing to the development of thermal-management technologies.

SUPPLEMENTARY MATERIAL

See the Supplementary Material for details of the X-ray diffraction pattern, the M-H curves, and the magnetic-field dependence of the Seebeck voltages of the FePt thin film.

ACKNOWLEDGMENTS

This work was partially supported by ERATO "Magnetic Thermal Management Materials" (Grant No. JPMJER2201) and A-STEP (Stage II, Full-scale type) (Grant No. JPMJTR253A) from JST, Japan; Grants-in-Aid for Scientific Research (C) (KAKENHI; Grant No. 25K08463) from JSPS, Japan; ARIM of MEXT (JPMXP1225NM5220); and SEMITEC corporation.

DATA AVAILABILITY

The data that supports the findings of this study are available from the corresponding author upon reasonable request.

REFERENCES

[1]G. E. W. Bauer, E. Saitoh, and B. J. van Wees, Nat. Mater. **11**, 391 (2012).

[2]Y. Sakuraba, K. Hasegawa, M. Mizuguchi, T. Kubota, S. Mizukami, T. Miyazaki, and K. Takanashi, Appl. Phys. Express **6**, 033003 (2013).

[3]S. R. Boona, R. C. Myers, and J. P. Heremans, Energy Environ. Sci. **7**, 885 (2014).

[4]Y. Sakuraba, Scr. Mater. **111**, 29 (2016).

[5]M. Ikhlas, T. Tomita, T. Koretsune, M.-T. Suzuki, D. Nishio-Hamane, R. Arita, Y. Otani, and S. Nakatsuji, Nat. Phys. **13**, 1085 (2017).

[6]S. N. Guin, P. Vir, Y. Zhang, N. Kumar, S. J. Watzman, C. Fu, E. Liu, K. Manna, W. Schnelle, J. Gooth, C. Shekhar, Y. Sun, and C. Felser, Adv. Mater. **31**, 1806622 (2019).

[7]K. Uchida, W. Zhou, and Y. Sakuraba, Appl. Phys. Lett. **118**, 140504 (2021).

[8]S. R. Boona, H. Jin, and S. Watzman, J. Appl. Phys. **130**, 171101 (2021).

[9]S. Liu, M. Chen, C. Fu, and T. Zhu, Adv. Phys. Res. **2**, 2300015 (2023).

[10]H. Adachi, F. Ando, T. Hirai, R. Modak, M. A. Grayson, and K. Uchida, Appl. Phys. Express **18**, 090101 (2025).

[11]A. Chanda, N. Schulz, R. R. Chowdhury, M.-H. Phan, and H. Srikanth, J. Phys.: Condens. Matter **37**, 473007 (2025).

[12]W. Zhou and Y. Sakuraba, Appl. Phys. Express **13**, 043001 (2020).

[13]T. Higo, Y. Li, K. Kondou, D. Qu, M. Ikhlas, R. Uesugi, D. Nishio-Hamane, C. L. Chien, Y. Otani, and S. Nakatsuji, Adv. Funct. Mater. **31**, 2008971 (2021).

[14]R. Modak, Y. Sakuraba, T. Hirai, T. Yagi, H. Sepehri-Amin, W. Zhou, H. Masuda, T. Seki, K. Takanashi, T. Ohkubo, and K. Uchida, Sci. Technol. Adv. Mater. **23**, 767 (2022).

[15]H. Tanaka, T. Higo, R. Uesugi, K. Yamagata, Y. Nakanishi, H. Machinaga, and S. Nakatsuji, Adv. Mater. **35**, 2303416 (2023).

[16]M. Odagiri, H. Imaeda, A. Yagmur, Y. Kurokawa, S. Sumi, H. Awano, and K. Tanabe, Sci. Rep. **14**, 17205 (2024).

[17]K. Hasegawa, M. Mizuguchi, Y. Sakuraba, T. Kamada, T. Kojima, T. Kubota, S. Mizukami, T. Miyazaki, and K. Takanashi, Appl. Phys. Lett. **106**, 252405 (2015).

[18]W. Zhou, K. Masuda, and Y. Sakuraba, Appl. Phys. Lett. **118**, 152406 (2021).

[19]R. Liu, L. Cai, T. Xu, J. Liu, Y. Cheng, and W. Jiang, Appl. Phys. Lett. **122**, 022406 (2023).

[20]S. Noguchi, K. Fujiwara, Y. Yanagi, M.-T. Suzuki, T. Hirai, T. Seki, K. Uchida, and A. Tsukazaki, Nat. Phys. **20**, 254 (2024).

[21]K. Ito, T. Kubota, and K. Takanashi, Phys. Rev. Applied. **21**, 054012 (2024).

[22]H. Yu, S. J. Park, I. Lee, J. H. Shim, and H. Jin, Sci. Technol. Adv. Mater. **26**, 2544649 (2025).

[23]T. Böhnert, V. Vega, A. Michel, V. M. Prida, and K. Nielsch, Appl. Phys. Lett. **103**, 092407 (2013).

[24]T. Hirai, R. Modak, A. Miura, T. Seki, K. Takanashi, and K. Uchida, Appl. Phys. Express **14**, 073001 (2021).

[25]J. Wang, A. Miura, R. Modak, Y. K. Takahashi, and K. Uchida, Sci. Rep. **11**, 11228 (2021).

[26]J. A. D. Sousa, E. Sánchez-Villegas, and C. O. Avci, Adv. Mater. Technol. **10**, e00770 (2025).

[27]M. H. Kryder, E. C. Gage, T. W. McDaniel, W. A. Challener, R. E. Rottmayer, G. Ju, Y.-T. Hsia, and M. F. Erden, Proc. IEEE **96**, 1810 (2008).

[28]D. Weller, G. Parker, O. Mosendz, A. Lyberatos, D. Mitin, N. Y. Safonova, and M. Albrecht, J. Vac. Sci. Technol. B **34**, 060801 (2016).

[29]R. F. C. Farrow, D. Weller, R. F. Marks, M. F. Toney, D. J. Smith, and M. R. McCartney, J. Appl. Phys. **84**, 934 (1998).

[30]T. Seki, T. Shima, K. Takanashi, Y. Takahashi, E. Matsubara, and K. Hono, IEEE Trans. Magn. **40**, 2522 (2004).